Mautner VF, Stephani U, Tassinari CA, Moschonas NK, Siebert R, Lopez de Munain A, Perez-Tur J, Nobile C: Autosomal dominant lateral temporal epilepsy: clinical spectrum, new epitempin mutations, and genetic heterogeneity in seven European families. *Epilepsia* 44: 1289–1297, 2003

14) Mihara T, Baba K: Combined use of subdural and depth electrodes, *in* Luders HO, Comair YG (*eds*): *Epilepsy Surgery, 2nd ed.* Philadelphia, Lippincott Williams & Wilkins, 2001, pp 613–621

15) Morante-Redolat JM, Gorostidi-Pagola A, Piquer-Sirerol S, Saenz A, Poza JJ, Galan J, Gesk S, Sarafidou T, Mautner VF, Binelli S, Staub E, Hinzmann B, French L, Prud'homme JF, Passarelli D, Scannapieco P, Tassinari CA, Avanzini G, Marti-Masso JF, Kluwe L, Deloukas P, Moschonas NK, Michelucci R, Siebert R, Nobile C, Perez-Tur J, Lopez de Munain A: Mutations in the LGI1/Epitempin gene on 10q24 cause autosomal dominant lateral temporal epilepsy. *Hum Mol Genet* 11: 1119–1128, 2002

16) Ottman R, Risch N, Hauser WA, Pedley TA, Lee JH, Barker-Cummings C, Lustenberger A, Nagle KJ, Lee KS, Scheuer ML, Neystat M, Susser M, Wilhelmsen KC: Localization of a gene for partial epilepsy to chromosome 10q. *Nat Genet* 10: 56–60, 1995

17) Pacia SV, Devinsky O, Perrine K, Ravdin L, Luciano D, Vazquez B, Doyle WK: Clinical features of neocortical temporal lobe epilepsy. *Ann Neurol* 40: 724–730, 1996

18) Pacia SV, Ebersole JS: Intracranial EEG substrates of scalp ictal patterns from temporal lobe foci. *Epilepsia* 38: 642–654, 1997

19) Shimizu H, Kawai K, Sunaga S, Sugano H, Yamada T: Hippocampal transection for treatment of left temporal lobe epilepsy with preservation of verbal memory. *J Clin Neurosci* 13: 322–328, 2006

20) Shimizu H, Suzuki I, Ohta Y, Ishijima B: Mesial temporal subdural electrode as a substitute for depth electrode. *Surg Neurol* 38: 186–191, 1992

21) Striano P, Gambardella A, Coppola A, Di Bonaventura C, Bovo G, Diani E, Boaretto F, Egeo G, Ciampa C, Labate A, Testoni S, Passarelli D, Manna I, Sferro C, Aguglia U, Caranci F, Giallonardo AT, Striano S, Nobile C, Michelucci R: Familial mesial temporal lobe epilepsy (FMTLE): a clinical and genetic study of 15 Italian families. *J Neurol* 255: 16–23, 2008

Address reprint requests to: Kensuke Kawai, MD, DMSc, Department of Neurosurgery, Graduate School of Medicine, the University of Tokyo, 7-3-1 Hongo, Bunkyo-ku, Tokyo 113-9655, Japan.
e-mail: kenkawai-tky@umin.ac.jp

A Detailed Analysis of Functional Magnetic Resonance Imaging in the Frontal Language Area: A Comparative Study With Extraoperative Electrocortical Stimulation

Naoto Kunii, MD*
Kyousuke Kamada, MD, PhD*‡
Takahiro Ota, MD, PhD*
Kensuke Kawai, MD, PhD*
Nobuhito Saito, MD, PhD*

*Department of Neurosurgery, University of Tokyo, Tokyo, Japan. ‡Now at the Department of Neurosurgery, Asahikawa Medical University, Asahikawa, Japan

Correspondence:
Kyousuke Kamada, MD, PhD,
Department of Neurosurgery,
Asahikawa Medical University,
Asahikawa, Japan, 2-1,
Midorigaoka-Higashi,
Asahikawa, Hokkaido 078-8510, Japan.
E-mail: kamady-k@umin.ac.jp

Received, August 30, 2010.
Accepted, February 2, 2011.
Published Online, March 23, 2011.

BACKGROUND: Functional magnetic resonance imaging (fMRI) is a less invasive way of mapping brain functions. The reliability of fMRI for localizing language-related function is yet to be determined.

OBJECTIVE: We performed a detailed analysis of language fMRI reliability by comparing the results of 3-T fMRI with maps determined by extraoperative electrocortical stimulation (ECS).

METHODS: This study was performed on 8 epileptic patients who underwent subdural electrode placement. The tasks performed during fMRI included verb generation, abstract/concrete categorization, and picture naming. We focused on the frontal lobe, which was effectively activated by these tasks. In extraoperative ECS, 4 tasks were combined to determine the eloquent areas: spontaneous speech, picture naming, reading, and comprehension. We calculated the sensitivity and specificity with different *Z* score thresholds for each task and appropriate matching criteria. For further analysis, we divided the frontal lobe into 5 areas and investigated intergyrus variations in sensitivity and specificity.

RESULTS: The abstract/concrete categorization task was the most sensitive and specific task in fMRI, whereas the picture naming task detected eloquent areas most efficiently in ECS. The combination of the abstract/concrete categorization task and a 3-mm matching criterion gave the best tradeoff (sensitivity, 83%; specificity, 61%) when the *Z* score was 2.24. As for intergyrus variation, the posterior inferior frontal gyrus showed the best tradeoff (sensitivity, 91%; specificity, 59%), whereas the anterior middle frontal gyrus had low specificity.

CONCLUSION: Despite different tasks for fMRI and extraoperative ECS, the relatively low specificity might be caused by a fundamental discrepancy between the 2 techniques. Reliability of language fMRI activation might differ, depending on the brain region.

KEY WORDS: Electrocortical stimulation, Functional MRI, Language, Sensitivity, Specificity

Neurosurgery 69:590–597, 2011 DOI: 10.1227/NEU.0b013e3182181be1 www.neurosurgery-online.com

ABBREVIATIONS: AC, abstract/concrete categorization; **DICOM,** digital imaging and communications in medicine; **ECS,** electrocortical stimulation; **eoECS,** extraoperative electrocortical stimulation; **fMRI,** functional magnetic resonance imaging; **IFG,** inferior frontal gyrus; **MFG,** middle frontal gyrus; **PN,** picture naming; **ROC,** receiver-operating characteristics; **VG, verb generation**

Functional magnetic resonance imaging (fMRI) is used to identify the dominant hemisphere of language-related functions and has been applied to clinical practice.[1-6] The localization reliability of fMRI during language tasks (language fMRI) has received a great deal of attention because of the invasiveness of electrocortical stimulation (ECS).

Although previous studies have calculated the sensitivity and specificity of language fMRI using

intraoperative ECS,[7-12] considerable disagreement remains between the sensitivity and specificity values calculated in each study.[13] Differences in results are contributed to, among other things, the different brain lesions treated in the studies. For example, whereas blood oxygen level–dependent fMRI might have risks of failure in functional mapping in several pathological brain conditions such as brain edema and high-grade gliomas,[14,15] epilepsy patients generally have no brain lesions in the frontal lobe and are relatively appropriate for fMRI-ECS study. The inconsistency also is derived from differences in the validation methods used in each study and the variety of language tasks performed during fMRI sessions and the intraoperative ECS procedure. In particular, it is hard to examine all of the exposed cortical areas thoroughly by intraoperative ECS owing to operative time restrictions and the number of language tasks that can be performed during awake procedures. We assumed that a considerable part of the inconsistent findings of previous studies arose from the technical limitations of intraoperative ECS.

Our question is whether extraoperative ECS (eoECS) with multiple language tasks would result in a better correlation with high-field fMRI findings. Use of subdural electrodes allowed us to meticulously examine the extensive brain areas and intergyrus variation of fMRI reliability. We focused on the frontal language area because the frontal lobe is more dominantly activated by semantic tasks.[4,6]

SUBJECTS AND METHODS

Patients

Functional brain mapping with both language fMRI and eoECS has been performed at the University of Tokyo Hospital in 12 patients with intractable epilepsy since December 2006, when a 3-T MRI scanner was installed. We implanted subdural grid electrodes for diagnostic purposes and obtained 3-dimensional (3D) head computed tomography (CT) scans that delineated the electrode profiles for all patients. Four patients were excluded because they had a low intelligence quotient (< 70) or because none of the implanted electrodes covered the inferior or middle frontal lobe. As a result, we investigated 8 patients (3 men, 5 women). Detailed demographic data are shown in Table 1. Before epilepsy surgery, we confirmed the dominant cerebral hemisphere for language functions using the Wada test. Seven patients showed left language dominance, and 1 expressed impairment of spontaneous speech in each hemispheric examination, suggesting bilateral language lateralization. The final analyses were performed on 9 hemispheres in 8 patients in whom we compared language fMRI with eoECS. This study was approved by the institutional review board of our institute. Written informed consent was obtained from each patient or the family before participation in the study.

TABLE 1. Demographic Data of the Patients[a]

Patient	Age, y/ Sex	Diagnosis	Language Dominance	VIQ Score	Electrodes, n
1	50/F	R TLE, cavernous malformation	L	91	30
2	40/M	L TLE	L	85	24
3	33/F	L FLE, L TLE	L	94	32
4	40/M	R TLE	L	93	21
5	35/F	L TLE	L	107	20
6	21/M	L TLE	L	79	20
7	36/F	L TLE	L	72	29
8	31/F	R TLE	Bilateral	86	L 25, R 21

[a]FLE, frontal lobe epilepsy; TLE, temporal lobe epilepsy; VIQ, Verbal Intelligence Quotient in the Wechsler Adult Intelligence Scale, revised.

Language fMRI

We performed MRI using a 3-T MR scanner with echo-planar capabilities and a whole-head receive-only coil (Signa, General Electric). During the experiments, foam cushions were used to immobilize the patient's head. Before the fMRI session, 3D T1-weighted MRIs of the subject's brain were obtained, which consisted of 136 sequential 1.4-mm-thick axial slices with a resolution of 256 × 256 pixels in a field of view of 240 mm. We performed fMRI with a T2*-weighted echo-planar imaging sequence (echo time, 35 ms; repetition time, 4000 ms; flip angle, 90°; slice thickness, 4 mm; slice gap, 1 mm; field of view, 280 mm; matrix, 64 × 64; number of slices, 22). Because of the different head sizes and positions of the patients, we selected a large field of view that would always be able to contain the entire head, fixing the same center of the field of view on the *x* and *y* axes for all sessions. This enabled simple and exact coregistration of the different image sessions.

Each fMRI session consisted of 3 dummy scan volumes, 3 activation periods, and 4 baseline (rest) periods. During each period, 5 echo-planar imaging volumes were collected, yielding a total of 38 imaging volumes. Language fMRI data were acquired as follows. All subjects were examined with 3 different semantic language paradigms: verb generation (VG) by listening to nouns, abstract/concrete categorization (AC) by reading words, and naming presented pictures (PN). All words for the semantic tasks were selected from common Japanese words listed in the electronic dictionary produced by the National Institute for Japanese Language.

VG Task

For the auditory stimuli (duration range was within 500 milliseconds), common concrete nouns spoken by a native Japanese speaker were delivered binaurally via MR-compatible headphones. Backward playback of the sound files (reference sounds) was used to eliminate primary auditory activation during the rest periods with the same interstimulus intervals (1600-2400 milliseconds) as the active periods. The subjects were instructed to silently generate a verb related to each presented noun during the active periods and to passively listen to the reference sounds during the rest periods.

AC Task

Visual stimuli were presented on a liquid crystal display monitor, with a mirror above the head coil allowing the patient to see the stimuli. In the active periods, words consisting of 3 Japanese letters were presented in a 2000-millisecond exposure time with interstimulus intervals of 500 milliseconds. The patients were instructed to categorize the presented word silently into "abstract" or "concrete" on the basis of the nature of the word. During the rest periods, the patients passively viewed random dots of destructured letters that had the same luminance as the stimuli to eliminate primary visual responses.

PN Task

In the same setting as the AC task, color illustrations of familiar objects were presented in a 2000-millisecond exposure time with interstimulus intervals of 500 milliseconds, and the patients were instructed to silently name the objects. During the rest periods, the patients passively viewed destructured illustrations with the same luminance as the stimuli shown in the active periods.

Functional data sets were realigned with a 3D motion correction program and were smoothed with a 10-mm basic filter. Functional activation maps were obtained by estimating the Z scores between the rest and activation periods using Dr View (Asahi Kasei, Tokyo, Japan).[1] To compare the results with eoECS mapping, we selected 4 different Z scores of 1.65, 1.96, 2.24, and 2.58, which corresponded to 2-sided P values of .1, .05, .025 and .01, respectively.

eoECS Study

The long-term subdural electrodes used consisted of Silastic sheets embedded with platinum electrodes (3 mm in diameter) with a 10-mm interelectrode interval (center to center; Unique Medical, Tokyo, Japan). We performed the examination at least 5 days after the implantation of the subdural electrodes and used 4 lexical semantic language tasks: spontaneous speech, picture naming, reading, and comprehension. During the eoECS mapping, the subject sat on a bed with a reclining backrest in a quiet, electrically shielded room. In the spontaneous speech task, the patients were asked to say their address and birthday in sequence. For the picture naming and reading tasks, the subjects were instructed to name the presented illustrations and to read the presented words aloud, respectively. In the comprehension task, we showed 6 simple graphic symbols and asked the patient to point to the symbol that we verbally described.

Constant current electric stimulation was delivered to pairs of electrodes with an electric stimulator (KS-101; Unique Medical Inc) with 5-second trains of 50-Hz, 0.2-millisecond alternating-polarity square-wave pulses. The stimulus intensity started at 4 mA and increased in 2-mA increments up to a maximum of 12 mA. While the stimulus intensity was increased, 4 experienced neurosurgeons evaluated the disruption of language-related functions.

When stimulation with an electrode pair reproducibly induced disruption of language-related functions such as speech arrest, hesitation, semantic paranomia, perseveration, or difficulty in comprehension, both electrodes were indicated to be positive. If the maximum stimulus intensity induced no impairment, we decided that the electrode pair was negative.

Comparison of eoECS and fMRI

To compare language fMRI results with eoECS mapping, we created 3D lateral views of the investigated hemispheres, which elucidated the spatial relationships between fMRI activation and all electrode positions (Figure 1A).

We elaborated the brain surface images by integrating 3D CT, 3D MRI, and fMRI in the following way. Because all MRIs were obtained during the same MR investigation using the same image center on the x and y axes, integration of the functional and anatomic data was performed by adjusting the z axis center of all sessions. We coregistered the 3D CT with the 3D MRI by maximizing the mutual information of both data sets. Then, the coregistered fMRI and 3D CT data were interpolated and resliced on the basis of 3D MRI. The brain surface data of all patients were semiautomatically extracted by Dr View. The

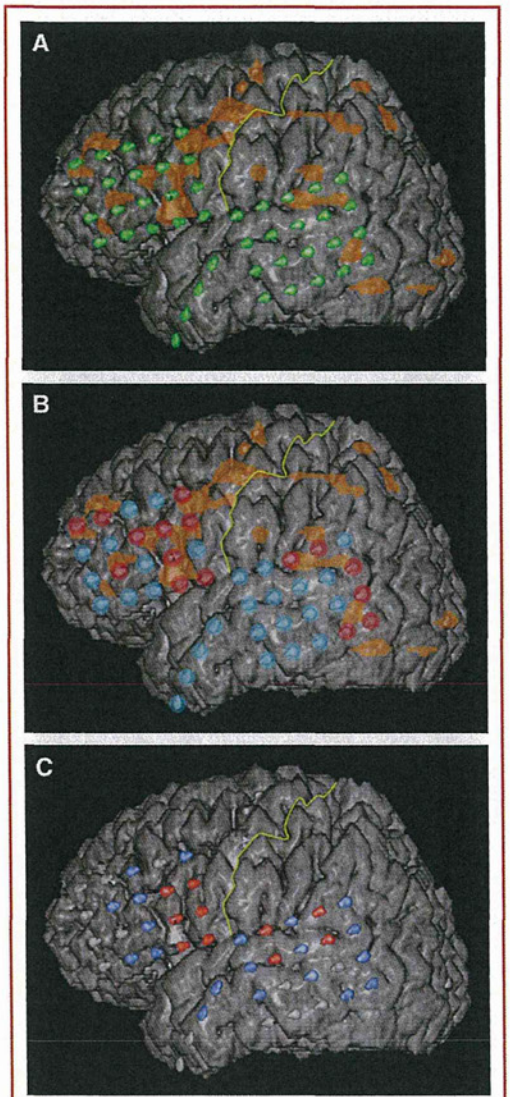

FIGURE 1. *Fused images produced by anatomic MRI, functional MRI (fMRI), and subdural electrodes.* **A**, *a fused image showing fMRI activation induced by the abstract/concrete categorization (AC) task ($Z > 2.24$, orange) and electrodes (green). Note that more activation was found in the frontal lobe than in the temporoparietal areas.* **B**, *electrodes with 6-mm matching criterion. The electrodes involved in fMRI activation [fMRI(+)] are indicated in red; the fMRI(−) electrodes are blue.* **C**, *electrodes for electrocortical stimulation (ECS). The electrodes that disrupted language-related functions (positive) are indicated in red. The blue electrodes were negative for ECS.*

extracted the 3D MRI and resliced data sets of 3D CT and fMRI were imported into RealIntage (KGT) in digital imaging and communications in medicine (DICOM) format for 3D reconstruction. Integrated and reconstructed brain surface images delineated the electrodes, language fMRI activation, and cortical structures.

To focus on the frontal language functions, we excluded the electrodes on the precentral gyrus when calculating the sensitivity and specificity of the language fMRI. We virtually defined 2 electrode diameters of 3 and 6 mm (matching criteria) to judge whether there was a match between an electrode and fMRI activation. These conservative matching criteria were selected on the basis of the reported effective diameter of bipolar cortical stimulation and to avoid oversampling of the effects of stimulation.[9]

All electrodes were classified into 4 groups according to whether the matching criteria of each electrode involved any fMRI activation [fMRI(+) or fMRI(−)] and/or whether each electrode was positive (+) or negative (−) on ECS (Figure 1B and 1C). Using these 4 electrode groups, we obtained the sensitivity and specificity as follows: sensitivity = fMRI(+) + ECS(+) / ECS(+) and specificity = fMRI(−) + ECS(−)/ ECS(−). By comparing the results of the 3 language fMRI tasks and 2 different matching criteria, we estimated receiver-operating characteristics (ROC) curves and found the best tradeoff by maximizing the Youden Index. We calculated the Youden Index by subtracting 1 from the sum of sensitivity and specificity at a point of interest, which indicated the vertical distance between each plot and the diagonal line.[16-18]

Spatial Variations in the Sensitivity/Specificity of the Frontal Lobe

We used the condition with the maximum Youden Index in each patient for further analysis of sensitivity and specificity in the frontal lobe, which was anatomically divided into 5 areas: the precentral gyrus, anterior and posterior middle frontal gyrus (MFG), and anterior and posterior inferior frontal gyrus (IFG). The anterior/posterior border was defined by drawing a line perpendicular to the Sylvian fissure from a point 2 cm anterior to the central sulcus (Figure 2). We calculated the sensitivity and specificity for each area using the language task, matching criteria, and Z score that gave the maximum Youden Index.

RESULTS

fMRI Results

The VG and PN tasks failed to identify language dominance in 3 cases. However, the AC task successfully indicated dominance and showed the most activated pixels in the frontal language area in all cases. The case involving bilateral representation demonstrated obvious activation in both frontal lobes. The temporal and parietal lobes showed less activation than the frontal lobe during all language tasks.

Because of the variation in the fMRI activation induced by each task, we selected 3 different Z scores of 1.96, 2.24, and 2.58 for the AC task and 1.65, 1.96, and 2.24 for the VG and PN tasks.

ECS Results

We analyzed 107 electrodes that were implanted in 9 frontal lobes with language representation. The mean ± SD of electrode number for each hemisphere was 12 ± 3.3. Among 44 ECS(+) electrodes (41%), impairment of picture naming and spontaneous speech was induced by ECS in 40 (91%) and 30 (68%) electrodes, respectively. These tasks found more ECS(+) electrodes compared with the reading or comprehension task.

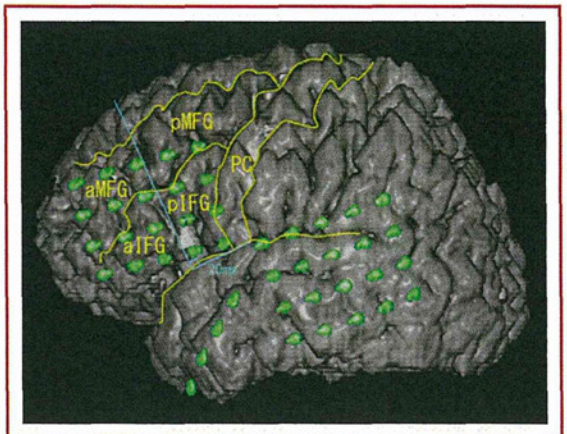

FIGURE 2. *Defined brain regions in the frontal language areas, which consisted of 3 gyri: the precentral gyrus (PC), middle frontal gyrus (MFG), and inferior frontal gyrus (IFG). The anterior/posterior border was defined by drawing a line (blue line) perpendicular to the Sylvian fissure from a point 2 cm anterior to the central sulcus. Thus, IFG and MFG were divided into anterior (aIFG and aMFG) and posterior (pIFG and pMFG) sections.*

Comparison Between fMRI and ECS Mapping Results

By changing the Z score of fMRI, we calculated the sensitivity and specificity for each task and matching criteria (Table 2), and the obtained sensitivity and specificity of various Z scores were plotted for each task to produce ROC curves (Figure 3). The ROC curves for the AC task had consistently higher sensitivity and lower false-positive values, indicating that the AC task was superior to others with regard to the efficient identification of ECS(+) areas. On the other hand, changing the matching criterion from 3 to 6 mm did not significantly affect the ROC curves.

The Youden Index is a simple approach for minimizing error that is equivalent to maximizing the sum of the sensitivity and specificity. The maximum Youden Index (0.44) was found at a Z score of 2.24 on the ROC curve for the AC task with a matching criterion of 3 mm. This score provided the best tradeoff between sensitivity (0.83) and specificity (0.61).

Intergyrus Differences in fMRI Reliability

We calculated the sensitivity and specificity for each gyrus under the conditions with the best tradeoff (task, AC; matching criterion, 3 mm; Z score, 2.24; Table 3). The posterior sections of the IFG and MFG showed better sensitivity and specificity than the anterior parts. In particular, the posterior IFG showed 91% sensitivity and 59% specificity, providing the maximum Youden Index.

However, the precentral gyrus demonstrated values of 50% for both measures, suggesting that fMRI activation in the gyrus

TABLE 2. Sensitivity and Specificity in Different Tasks and Analysis Parameters[a]

	Matching Criterion = 3 mm				Matching Criterion = 6 mm			
	Z Score				Z Score			
	1.65	1.96	2.24	2.58	1.65	1.96	2.24	2.58
AC task								
Sensitivity, %		90	83	76		100	93	86
Specificity, %		52	61	68		31	47	56
VG task								
Sensitivity, %	64	39	33		76	55	42	
Specificity, %	19	38	53		16	19	41	
PN task								
Sensitivity, %	70	60	55		90	75	65	
Specificity, %	41	53	53		26	44	47	

[a]AC, abstract/concrete categorization; PN, picture naming; VG, verb generation.

provides little information for ECS mapping, even under optimal conditions. The anterior MFG had a notably low specificity compared with other language areas, reducing the overall specificity of this study.

DISCUSSION

We achieved detailed analysis of the frontal language area by comparing language fMRI performed with a 3-T MR scanner and eoECS performed with subdural electrodes. The analysis

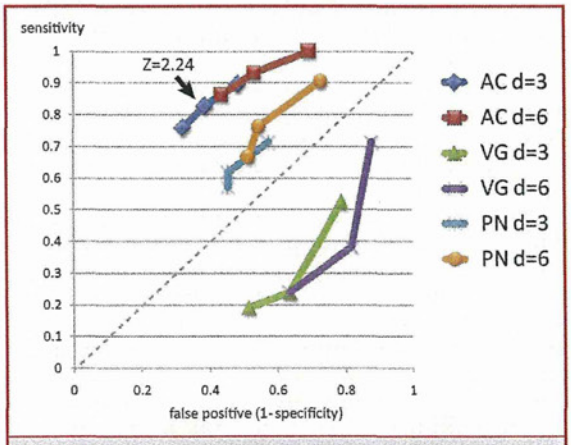

FIGURE 3. *Receiver-operating characteristic (ROC) curves for 6 different combinations of 3 tasks (abstract/concrete categorization [AC], verb generation [VG], and picture naming [PN]) and 2 matching criteria (electrode diameter [d] = 3 and 6 mm). The ROC curves were obtained by plotting sensitivity on the vertical axis and true positive value (1− specificity) on the horizontal axis. A point (Z score of 2.24) on the ROC curve for the AC task (3-mm matching criteria) gave the best tradeoff, as indicated by the arrow.*

TABLE 3. Sensitivity and Specificity of Each Gyrus in the Best Condition[a]

	PC	aMFG	pMFG	aIFG	pIFG
Sensitivity, %	50	80	80	75	91
Specificity, %	50	46	70	68	59

[a]aIFG, anterior inferior frontal gyrus; aMFG, anterior middle frontal gyrus; PC, precentral gyrus; pIFG, posterior inferior frontal gyrus; pMFG, posterior middle frontal gyrus.

conditions of the AC task, a Z score of 2.24, and matching criterion of 3 mm provided the best tradeoff (83% sensitivity, 61% specificity). Because of the high sensitivity, language fMRI could play a supportive role to determine priority order in ECS mapping. The posterior IFG demonstrated very high sensitivity, whereas the anterior MFG showed quite low specificity, suggesting that the gradation of language function occurs in each gyrus.

This study is unique in that we combined high-field fMRI and eoECS with multiple tasks. Five reports have investigated the sensitivity and specificity of language fMRI by ECS with awake craniotomy[7-10,12] (Table 4). Although most of them used a 1.5-T MR scanner and a PN task with awake craniotomy, their sensitivity and specificity values varied from 59% to 100% and 56% to 97%, respectively. One possible reason for these variable results is the inherent limitations of ECS such as the limits on investigation time and the number of available tasks. Therefore, we used eoECS and multiple semantic tasks and investigated patients in more comfortable conditions than awake craniotomy. In addition, the use of a higher magnetic field (3 T) allowed us to detect more blood oxygen level–dependent effects than a 1.5-T static magnetic field.[19,20] As a result, the best sensitivity and specificity were 91% and 59%, respectively. We confirmed that reading fMRI with a 3-T scanner is reliable and delivers high performance for ECS mapping. The high sensitivity allowed us to rapidly find the language centers during eoECS mapping and to understand the underlying brain network involved in language function. However, the use of a higher magnetic field does not automatically promise more reliable language maps because of other influencing factors.

On the other hand, we found that fMRI tended to overestimate the language-related brain areas, which were determined by eoECS in this study. As mentioned above, performing fMRI with a higher magnetic field might have produced better signal-to-noise ratios, presumably resulting in wider fMRI(+) regions. In addition, the low time resolution of fMRI merged various brain activations induced by semantic tasks. These limitations might have caused the low specificity observed in this study. To overcome this technical issue, it is necessary to increase the time resolution of language fMRI by using event-related fMRI and applying independent component analysis for postacquisition data analysis.[21] In addition, multiple comparisons among fMRI, eoECS, and functional prognosis should be done to find real eloquent areas for future study.

TABLE 4. Studies on the Agreement Between Functional Magnetic Resonance Imaging of Language Areas and Electrocortical Stimulation[a]

Series	Lesion Pathology	MFI, T	fMRI Task	ECS Task	Intraoperative/ Extraoperative ECS	Stimulation Sites in Each Lobe, n	Sensitivity/ Specificity, %
Fitzgerald et al,[12] 1997	Brain tumor	1.5	Reading,	Counting	Intraoperative	FTP 71	81/53-92/0 (listening)
			Vis VG	Reading			
						Listening	SS
			Aud VG	PN			
Pouratian et al,[10] 2002	Vascular malformation	3	PN	PN	Intraoperative	F 30, TP 69	100/67 (3 expressive tasks combined)
			Word generation				
			Aud responsive				
			Vis responsive				
			SC				
Rutten et al,[9] 2002	Epilepsy	1.5	Vis VG	PN	Intraoperative	TP 207	92/61 (all 4 tasks combined)
			PN				
			Verbal fluency				
			SC				
Roux et al,[8] 2003	Brain tumor	1.5	Vis VG	PN	Intraoperative	FTP 426	59/97 (VG + PN)
			PN				
Bizzi et al,[7] 2008	Brain tumor	1.5	Aud VG	ND	Intraoperative	FTP 141(F 70)	80/78 (VG)
Present study	Epilepsy	3	Reading	SS	Extraoperative	F 91	83/61 (Reading)

[a]Aud, auditory; ECS, electrocortical stimulation; F, frontal; fMRI, functional magnetic resonance imaging; MFI, magnetic field intensity; ND, not described; P, parietal; PN, picture/object naming; SC, sentence comprehension; SS, spontaneous speech; T, temporal; VG, verb generation; Vis, visual.

The picture naming task has been most widely used as a single task for language mapping in awake procedures. Meanwhile, the extraoperative condition allowed us to use multiple language tasks. To see whether the agreement between fMRI and ECS could be optimized when multiple tasks are combined, we reanalyzed our data using only the results of picture naming, which found > 90% of all the ECS(+) electrodes. We obtained ROC curves (data not shown) and the best tradeoff (sensitivity, 85%; specificity, 60%) similar to the results of multiple tasks. Contrary to our expectation, these findings suggested that multiple-task ECS does not necessarily result in better correlation with language fMRI. At least in part, a picture naming task might be practically most suitable to detect suppression of language related function by eoECS.

We divided the frontal lobe into 5 regions to obtain the best tradeoff because different symptoms were evoked by ECS within the IFG and MFG. As a result, we found that the anterior and posterior sections of the IFG had sensitivities of 75% and 91%, respectively. In addition, we found that most false fMRI activation occurred in the anterior MFG. It is important to know the sensitivity and specificity of the various brain regions. Previous reports investigated fMRI(+) regions by ECS with no anatomic information. Our study demonstrated that the reliability of language fMRI activation might differ, depending on the brain regions.

We used conservative matching criteria compared with previous studies. Rutten et al[9] suggested that conservative criteria might avoid oversampling of the effects of stimulation because the ECS electric current is quite localized and spreads only a few millimeters from the electrode.[22–24] We believe that these analysis criteria are suitable for comparisons of fMRI and ECS findings.

A potential limitation of this kind of study is the localization of the electrodes. We think the localization error of this study would be within the acceptable range. We focused only on the frontal language area, not on the temporal base or other brain regions, which were out of craniotomy or hidden by dura mater. In this analysis, 3 neurosurgeons confirmed that the electrode locations were almost the same as the MRI-CT fusion images by visual inspection.

Another limiting factor is the ambiguity in determining the positive electrodes. The stimulus was provided by alternative current, which might influence both electrodes. Therefore, it is necessary to stimulate each electrode at least twice in different combinations to know whether the electrode is truly responsible for the positive result. Instead of taking this approach, we considered each ambiguous electrode positive to avoid underestimation. This might be one of the technical limitations in this study. We should address the issue in future study.

A critical problem in this study was that we compared the results of activation (fMRI) and inhibition (ECS) mapping. To minimize this problem, we used eoECS with comfortable conditions and multiple tasks for both investigations. However, neither the sensitivity nor specificity reached 100%. Such an agreement will probably never be reached because of fundamental differences in outcome measures between the 2 methods.[25,26] We

have to keep in mind that our final goal is not to achieve an agreement between fMRI and ECS but to localize true language areas. It is well established that the use of different ECS tasks can lead to a different pattern of language areas, suggesting that ECS is a highly task-specific method. This also means that inadequate ECS can miss language areas. Even though we demonstrated that picture naming found language areas most efficiently, there is no guarantee that all eloquent areas were detected. In that sense, ECS is a tentative gold standard. We need to keep this point in mind when evaluating the results of ECS.

Our study demonstrated clinical usefulness of language-fMRI for eoECS mapping. The AC (reading) task was the best for language fMRI, and the high sensitivity of reading fMRI showed the possibility of shortening the whole investigation time of not only eoECS but also the awake procedure. This study sheds light on regional differences of reading fMRI reliability in the language-related areas. We need further verification with a larger sample size to clarify such an intergyrus variation of fMRI reliability. It is also necessary to investigate the temporal language areas with this technique.

A major question of fMRI studies is the discrepancy between the results of fMRI and ECS mapping. Recent electrocorticography (or magnetoencephalography) studies of brain oscillation such as event-related synchronization might help us interpret the underlying physiological mechanism of each technique.[27–31] Future research answering this question might improve the reliability of language fMRI, especially in low-specificity areas.

Disclosure

This work was supported in part by the Japan Epilepsy Research Foundation; Takeda Promotion of Science Foundation; grant-in-aid 21390406 for Scientific research from MEXT; grant-in-aid 21119508 for Scientific Research on Innovative Areas by the MEXT; a research grant for decoding and controlling brain information from Japan Science and Technology Agency; a research grant from the Princess Takamatsu Cancer Research Fund; and the Terumo Promotion of the Science Foundation. The authors have no personal financial or institutional interest in any of the drugs, materials, or devices described in this article.

REFERENCES

1. Kamada K, Sawamura Y, Takeuchi F, et al. Expressive and receptive language areas determined by a non-invasive reliable method using functional magnetic resonance imaging and magnetoencephalography. *Neurosurgery.* 2007;60(2):296-305.
2. Detre JA. fMRI: applications in epilepsy. *Epilepsia.* 2004;45(suppl 4):26-31.
3. Fernandez G, Specht K, Weis S, et al. Intrasubject reproducibility of presurgical language lateralization and mapping using fMRI. *Neurology.* 2003;60(6):969-975.
4. Lehericy S, Cohen L, Bazin B, et al. Functional MR evaluation of temporal and frontal language dominance compared with the Wada test. *Neurology.* 2000;54(8):1625-1633.
5. Binder JR, Swanson SJ, Hammeke TA, et al. Determination of language dominance using functional MRI: a comparison with the Wada test. *Neurology.* 1996;46(4): 978-984.
6. Desmond JE, Sum JM, Wagner AD, et al. Functional MRI measurement of language lateralization in Wada-tested patients. *Brain.* 1995;118(pt 6):1411-1419.
7. Bizzi A, Blasi V, Falini A, et al. Presurgical functional MR imaging of language and motor functions: validation with intraoperative electrocortical mapping. *Radiology.* 2008;248(2):579-589.
8. Roux FE, Boulanouar K, Lotterie JA, Mejdoubi M, LeSage JP, Berry I. Language functional magnetic resonance imaging in preoperative assessment of language areas: correlation with direct cortical stimulation. *Neurosurgery.* 2003;52(6):1335-1345.
9. Rutten GJ, Ramsey NF, van Rijen PC, Noordmans HJ, van Veelen CW. Development of a functional magnetic resonance imaging protocol for intraoperative localization of critical temporoparietal language areas. *Ann Neurol.* 2002;51(3):350-360.
10. Pouratian N, Bookheimer SY, Rex DE, Martin NA, Toga AW. Utility of preoperative functional magnetic resonance imaging for identifying language cortices in patients with vascular malformations. *J Neurosurg.* 2002;97(1):21-32.
11. Yetkin FZ, Mueller WM, Morris GL, et al. Functional MR activation correlated with intraoperative cortical mapping. *AJNR Am J Neuroradiol.* 1997;18(7):1311-1315.
12. FitzGerald DB, Cosgrove GR, Ronner S, et al. Location of language in the cortex: a comparison between functional MR imaging and electrocortical stimulation. *AJNR Am J Neuroradiol.* 1997;18(8):1529-1539.
13. Giussani C, Roux FE, Ojemann J, Sganzerla EP, Pirillo D, Papagno C. Is preoperative functional magnetic resonance imaging reliable for language areas mapping in brain tumor surgery? Review of language functional magnetic resonance imaging and direct cortical stimulation correlation studies. *Neurosurgery.* 2010;66(1):113-120.
14. Holodny AI, Schulder M, Liu WC, Wolko J, Maldjian JA, Kalnin AJ. The effect of brain tumors on BOLD functional MR imaging activation in the adjacent motor cortex: implications for image-guided neurosurgery. *AJNR Am J Neuroradiol.* 2000;21(8):1415-1422.
15. Holodny AI, Schulder M, Liu WC, Maldjian JA, Kalnin AJ. Decreased BOLD functional MR activation of the motor and sensory cortices adjacent to a glioblastoma multiforme: implications for image-guided neurosurgery. *AJNR Am J Neuroradiol.* 1999;20(4):609-612.
16. Mazaheri Y, Hricak H, Fine SW, et al. Prostate tumor volume measurement with combined T2-weighted imaging and diffusion-weighted MR: correlation with pathologic tumor volume. *Radiology.* 2009;252(2):449-457.
17. Fluss R, Faraggi D, Reiser B. Estimation of the Youden Index and its associated cutoff point. *Biom J.* 2005;47(4):458-472.
18. Youden WJ. Index for rating diagnostic tests. *Cancer.* 1950;3(1):32-35.
19. Scarabino T, Giannatempo GM, Popolizio T, et al. 3.0-T functional brain imaging: a 5-year experience. *Radiol Med.* 2007;112(1):97-112.
20. Ogawa S, Lee TM, Kay AR, Tank DW. Brain magnetic resonance imaging with contrast dependent on blood oxygenation. *Proc Natl Acad Sci U S A.* 1990;87(24):9868-9872.
21. McKeown MJ, Jung TP, Makeig S, et al. Spatially independent activity patterns in functional MRI data during the stroop color-naming task. *Proc Natl Acad Sci U S A.* 1998;95(3):803-810.
22. Gwinn RP, Spencer DD, Spencer SS, et al. Local spatial effect of 50 Hz cortical stimulation in humans. *Epilepsia.* 2008;49(9):1602-1610.
23. Nathan SS, Sinha SR, Gordon B, Lesser RP, Thakor NV. Determination of current density distributions generated by electrical stimulation of the human cerebral cortex. *Electroencephalogr Clin Neurophysiol.* 1993;86(3):183-192.
24. Haglund MM, Ojemann GA, Blasdel GG. Optical imaging of bipolar cortical stimulation. *J Neurosurg.* 1993;78(5):785-793.
25. Rutten GJ, Ramsey NF. The role of functional magnetic resonance imaging in brain surgery. *Neurosurg Focus.* 2010;28(2):E4.
26. Mandonnet E, Winkler PA, Duffau H. Direct electrical stimulation as an input gate into brain functional networks: principles, advantages and limitations. *Acta Neurochir (Wien).* 2010;152(2):185-193.
27. Edwards E, Nagarajan SS, Dalal SS, et al. Spatiotemporal imaging of cortical activation during verb generation and picture naming. *Neuroimage.* 2010;50(1):291-301.
28. Ojemann GA, Corina DP, Corrigan N, et al. Neuronal correlates of functional magnetic resonance imaging in human temporal cortex. *Brain.* 2010;133(pt 1):46-59.
29. Lachaux JP, Fonlupt P, Kahane P, et al. Relationship between task-related gamma oscillations and BOLD signal: new insights from combined fMRI and intracranial EEG. *Hum Brain Mapp.* 2007;28(12):1368-1375.
30. Sinai A, Bowers CW, Crainiceanu CM, et al. Electrocorticographic high gamma activity versus electrical cortical stimulation mapping of naming. *Brain.* 2005;128(pt 7):1556-1570.
31. Crone NE, Hao L, Hart J Jr, et al. Electrocorticographic gamma activity during word production in spoken and sign language. *Neurology.* 2001;57(11):2045-2053.

COMMENTS

The authors studied a battery of language tasks to increase the correlation between functional magnetic resonance imaging and stimulation mapping of anterior language sites. Frontal lobe activation

has been a reliable feature of many language studies, yet the authors can still demonstrate a gradient of correlation between the imaging and stimulation methods. The story for posterior language sites remains more complex, and these areas, despite obvious clinical importance, are not always evident in functional studies. Conversely, functional studies that do show temporal lobe activity use tasks that have not been used by clinical neurosurgery.[1] It is likely that such discrepancies have more to do with task selection than fundamental differences between the 2 mapping methods. Naming objects while sitting in the operating room can be disrupted but may not generate a large response, whereas the signal from relatively complicated language tasks may be quite diffuse but impractical for the operating room (or even extraoperative) setting. It does not mean that the 2 methods are somehow incompatible.

Jeffrey G. Ojemann
Seattle, Washington

1. Binder JR, Gross WL, Allendorfer JB, et al. Mapping anterior temporal lobe language areas with fMRI: a multicenter normative study. *Neuroimage*. 2011;54(2):1465-1475.

This is an original and important article owing to its goal of clarifying the reliability of the 2 techniques in neurosurgery, especially the affordability of language functional magnetic resonance imaging (fMRI) compared with the gold standard. In fact, a large amount of the recent neuropsychological literature accounts too much to fMRI studies without a quantification of the true sensitivity and specificity. This trend could be dangerous from clinical and legal points of view because of the frequently exaggerated expectancy of the surgeons and the patients for language fMRI to make surgery safer.

Several points in this article are interesting. It is important to underline the possibility of avoiding electrocortical stimulation in the areas where fMRI is negative owing to its high sensitivity. Moreover, I really appreciated the idea of verifying the sensitivity and specificity in different cortical frontal areas. These data, even if more investigation is needed, could be very important in surgical planning.

Even if electrocortical stimulation is still the gold standard, the role of fMRI is becoming more and more important. Therefore, we need to encourage studies that try to verify the reliability of emerging brain mapping techniques in neurosurgery.

Carlo Giussani
Monza, Italy

frontiers in
SYSTEMS NEUROSCIENCE

METHODS ARTICLE
published: 25 May 2011
doi: 10.3389/fnsys.2011.00034

Intrasulcal electrocorticography in macaque monkeys with minimally invasive neurosurgical protocols

Takeshi Matsuo[1,2†], Keisuke Kawasaki[1,3*†], Takahiro Osada[4], Hirohito Sawahata[1,3], Takafumi Suzuki[5], Masahiro Shibata[6], Naohisa Miyakawa[1,3], Kiyoshi Nakahara[7], Atsuhiko Iijima[1,3,8], Noboru Sato[6], Kensuke Kawai[2], Nobuhito Saito[2] and Isao Hasegawa[1,3*]

[1] Department of Physiology, Niigata University School of Medicine, Niigata, Japan
[2] Department of Neurosurgery, The University of Tokyo Graduate School of Medicine, Tokyo, Japan
[3] Center for Transdisciplinary Research, Niigata University School of Medicine, Niigata, Japan
[4] Department of Physiology, The University of Tokyo Graduate School of Medicine, Tokyo, Japan
[5] Graduate School of Information Science and Technology, The University of Tokyo, Tokyo, Japan
[6] Department of Anatomy, Niigata University School of Medicine, Niigata, Japan
[7] National Institute of Neuroscience, National Center of Neurology and Psychiatry, Tokyo, Japan
[8] Department of Biocybernetics, Graduate School of Science and Techology, Niigata University, Niigata, Japan

Edited by:
Raphael Pinaud, University of Oklahoma Health Sciences Center, USA

Reviewed by:
Hugo Merchant, Universidad Nacional Autónoma de México, Mexico
Takashi Yamamoto, Osaka University Graduate School of Dentistry, Japan

***Correspondence:**
Isao Hasegawa and Keisuke Kawasaki, Department of Physiology, Niigata University School of Medicine, Asahimachi Street 1-757, Chuo-ku, Niigata 951-8510, Japan.
e-mail: ihasegawa-nsu@umin.ac.jp; kkwasaki@med.niigata-u.ac.jp

†Takeshi Matsuo and Keisuke Kawasaki equally contributed to this work.

Electrocorticography (ECoG), multichannel brain-surface recording and stimulation with probe electrode arrays, has become a potent methodology not only for clinical neurosurgery but also for basic neuroscience using animal models. The highly evolved primate's brain has deep cerebral sulci, and both gyral and intrasulcal cortical regions have been implicated in important functional processes. However, direct experimental access is typically limited to gyral regions, since placing probes into sulci is difficult without damaging the surrounding tissues. Here we describe a novel methodology for intrasulcal ECoG in macaque monkeys. We designed and fabricated ultra-thin flexible probes for macaques with micro-electro-mechanical systems technology. We developed minimally invasive operative protocols to implant the probes by introducing cutting-edge devices for human neurosurgery. To evaluate the feasibility of intrasulcal ECoG, we conducted electrophysiological recording and stimulation experiments. First, we inserted parts of the Parylene-C-based probe into the superior temporal sulcus to compare visually evoked ECoG responses from the ventral bank of the sulcus with those from the surface of the inferior temporal cortex. Analyses of power spectral density and signal-to-noise ratio revealed that the quality of the ECoG signal was comparable inside and outside of the sulcus. Histological examination revealed no obvious physical damage in the implanted areas. Second, we placed a modified silicone ECoG probe into the central sulcus and also on the surface of the precentral gyrus for stimulation. Thresholds for muscle twitching were significantly lower during intrasulcal stimulation compared to gyral stimulation. These results demonstrate the feasibility of intrasulcal ECoG in macaques. The novel methodology proposed here opens up a new frontier in neuroscience research, enabling the direct measurement and manipulation of electrical activity in the whole brain.

Keywords: electrocorticography, sulcus, intrasulcal, monkey, MEMS, neurosurgery

INTRODUCTION

Cerebral cortex is intricately folded in many primate species. In humans, two-thirds of the cerebral cortex is buried in grooves, known as the cerebral sulci, whereas only one-third of the cortex is exposed in the cerebral gyri (Ribas, 2010). Similarly, in macaque monkeys, approximately half of the neocortex lies within the cerebral sulci (Felleman and Van Essen, 1991). Functional magnetic resonance imaging (fMRI) and positron emission tomography have revealed neural activation related to important functions such as cognition and attention in intrasulcal as well as gyral regions of the cerebral cortex (Tsao et al., 2003; Beauchamp et al., 2004; Koyama et al., 2004). These neuroimaging techniques, however, have difficulty obtaining precise spatiotemporal profiles of intrasulcal activity simultaneously with millimeter source localization and millisecond temporal resolution. On the other hand, extracellular spike recording is a widely used tool for investigating cortical functions at the level of single neurons (Mountcastle, 1957). Extracellular single neuronal activities also provide an efficient input for driving artificial effectors of neuroprosthetics (Hatsopoulos and Donoghue, 2009). However, repeated intrasulcal penetration of the microelectrode (Tomita et al., 1999) inevitably cause unintended damage to the intervening brain tissues in the course of recording sessions over months. Furthermore, when the microelectrode was chronically implanted, neural signals might possibly be lost after long period of time due to the isolation of the electrode's tip by glial cells (Polikov et al., 2005). Ideally, direct access to the intrasulcal cortices without damaging the surrounding tissues could enable stable recording from and stimulation to these regions in physiological conditions, advancing our understanding of the fundamental cerebral functions *in situ*.

A promising candidate is electrocorticography (ECoG), which was originally developed as a clinical tool for monitoring and mapping during neurosurgery. ECoG is now recognized as a well-balanced

methodology for basic neurophysiological investigations (Leuthardt et al., 2006; Fisch et al., 2009; Liu et al., 2009; Rubehn et al., 2009). Compared to scalp electroencephalography, ECoG has much better signal fidelity and spatial resolution (Leuthardt et al., 2006; Miller et al., 2009; Slutzky et al., 2010; Toda et al., 2011). In addition, compared to microelectrode recordings, ECoG has the advantage of recording local field potentials (LFPs) less invasively, with superior long-term stability (Rubehn et al., 2009; Chao et al., 2010). Recently various frequency components of LFP have been implicated in carrying informative sensory, motor, and cognitive signals across brain regions (Buschman and Miller, 2007; Liu et al., 2009), which further emphasizes the importance of ECoG. Nonetheless, the placement of ECoG arrays is usually limited to the surface of the brain. One previous report described the placement of ECoG arrays within the bank of the human central sulcus (CS; Yanagisawa et al., 2009). However, intrasulcal ECoG recording/stimulation in macaque monkeys, the most prevailing animal model for investigation of cognitive brain functions, is technically demanding, since the brain volume in macaque is less than one-tenth that of humans. To achieve intrasulcal ECoG in macaques, highly interdisciplinary approaches combining neurosurgery, neuroengineering, and neurophysiology would be required.

In the current study, we sought to develop surgical protocols for placing custom-designed ECoG probes for electrophysiological recording and stimulation within the cerebral sulci of macaque monkeys. The utility of our method was tested in two experiments. First, we evaluated the feasibility of intrasulcal ECoG recording. We designed an ultra-thin ECoG probe for macaques using micro-electro-mechanical systems (MEMS) technology (Toda et al., 2011), and tested whether visually evoked ECoG signals could be reliably recorded from the ventral bank of the superior temporal sulcus (STS), comparable to the signals from the surface of the inferior temporal gyrus (ITG). Second, we attempted direct stimulation of the intrasulcal cortex using a modified clinical-use ECoG probe. We compared the stimulation thresholds for muscle twitch between intrasulcal and gyral regions in the primary motor cortex (M1).

MATERIALS AND METHODS

GENERAL SURGICAL PROCEDURES

Three male macaque monkeys (two *Macaca fuscata* and one *M. mulatta*), weighing 6–9 kg were used for the intrasulcal ECoG recording experiment, in accord with the NIH Guidelines for the Care and Use of Laboratory Animals. The experimental protocol was approved by the Niigata University Institutional Animal Care and Use Committee. After premedication with ketamine (50 mg/kg) and medetomidine (0.03 mg/kg), each animal was intubated with an endotracheal tube of 6 or 6.5 mm and connected to an artificial respirator (A.D.S.1000, Engler Engineering Corp., FL, USA). The venous line was secured using lactated Ringer's solution, and ceftriaxone (100 mg/kg) was dripped as a prophylactic antibiotic. Postoperatively, the monkeys received ketoprofen as an analgesic for 3 days, and antibiotics were continued for 1 week after surgery. Body temperature was maintained at 37°C using an electric heating mat. A vacuum fixing bed (Vacuform, B.u.W.Schmidt GmbH, Garbsen, Germany) was used to maintain the position of the body. Oxygen saturation, heart rate, and end-tidal CO_2 were continuously monitored (Surgi Vet, Smiths Medical PM Inc., London, UK) throughout surgery to adjust the levels of anesthesia. The skull was fixed with a three-point fastening device (Integra Co., NJ, USA) with a custom-downsized attachment for macaques (**Figure 1A**). In the intra-dural operation, we used a microscope (Ophthalmo-Stativ S22, Carl Zeiss Inc., Oberkochen, Germany) with a CMOS color camera (TS-CA-130MIII, MeCan Imaging Inc., Saitama, Japan).

For the intrasulcal stimulation experiment, three male macaque monkeys (two *M. fuscata* and one *M. mulatta*) weighing 6–9 kg were used. All surgical and experimental protocols were in full compliance with the regulations of The University of Tokyo School of Medicine and with the NIH Guidelines for the Care and Use of Laboratory Animals. Surgery was conducted in aseptic conditions under general anesthesia with sodium pentobarbital (5 mg/kg/h). The skull was fixed using a stereotactic frame (Narishige, Tokyo, Japan). Postoperatively, the monkeys received ketoprofen for 3 days as an analgesic, and ampicillin for 1 week as an antibiotic. We used a microscope (OPMI Sensera, Carl Zeiss Inc., Oberkochen, Germany) with a color video camera (DXC-C1, Sony Co., Tokyo, Japan) during microsurgery.

SKIN INCISION AND CRANIOTOMY

In the operation for ECoG recording, following an S-shaped incision (**Figure 1B**), we dissected the layer between the skin and the muscle. The muscle was retracted forward while the skin was retracted downward, to secure a sufficient operative field. The target location and the size of the craniotomy were determined by preoperative MRI. The size of the craniotomy was 35 mm × 25 mm, and the zygomatic arch was removed to facilitate the approach. Four burr holes were opened by a perforator [Primado (PD-PER), NSK, Tochigi, Japan] with an attachment for infants (DGR-OS Mini

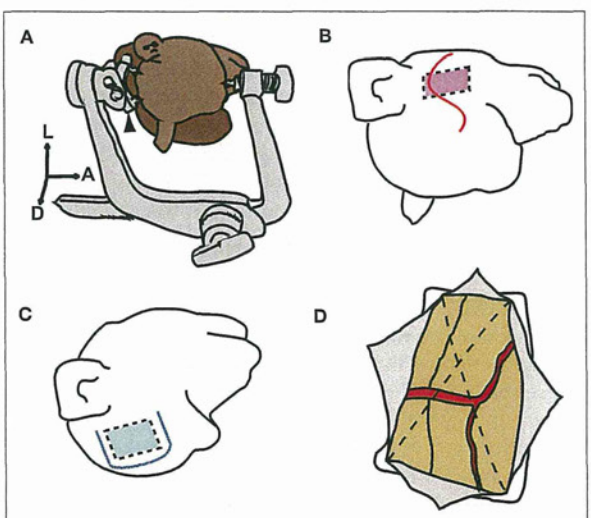

FIGURE 1 | Skull fixation and craniotomy. (A) Illustration of head positioning with a three-point fastening device. Black arrowhead indicates a customized attachment for macaques. A, anterior; L, left; D, dorsal. **(B)** S-shaped skin incision indicated by red line. Red rectangle indicates the range of the craniotomy for the superior temporal sulcus (STS). **(C)** U-shaped skin incision indicated by blue line. Blue square indicates the range of craniotomy for the central sulcus (CS). **(D)** Dural incision (dotted lines) into four quadrants. Each quadrant was retracted toward the margin of the craniotomy.

8/5 mm R, Acura-Cut Inc., MA, USA) (Movie S1 in Supplementary Material). After the bone and the dura mater were separated using an elevator, the skull was cut with a craniotome [Primado (PD-CRA), NSK, Tochigi, Japan], and the bone flap was removed. The range of craniotomy on the ventral edge was expanded by luer bone rongeur. Hemorrhage from the dura was controlled by a bipolar coagulator (Bipolar SX-2001, Tagawa Electronic Research Institute, Chiba, Japan). During the operation of the monkeys for the ECoG stimulation experiment, after a U-shaped skin incision (**Figure 1C**), a 30 mm × 35 mm craniotomy was made by drilling.

DURAL INCISION

We cut the dura mater in two steps. Initially, we cut the surface layer of the dura with a 21-gage injection needle. We then raised the edge of the surface layer and cut the lower layer of the dura. The subdural space was secured by raising up the whole dura layer. To prevent cortical damage, we inserted surgical cotton sheets (Bemsheets, Kawamoto Co., Osaka, Japan) into the subdural space. The dura was cut with scissors into four quadrants (**Figure 1D**), each of which was then retracted toward the margins of the craniotomy. Thus, oozing from the epidural space was effectively stopped and the operative field was kept clear throughout the operation.

INTRA-DURAL MICROSURGERY

All of the cortical surfaces except for the target sulcus were covered with wet surgical cotton sheets to prevent mechanical damage or drying. We used surgical cotton sheets or absorbable gelatin sponge (Gelfoam, Pfizer, NY, USA) as cushioning material between the surgical devices and brain tissue. We cut the surface arachnoid membrane near the blood vessel, utilizing the perivascular space (**Figure 2A**). A 27-gage injection needle (**Figure 2B**) was suitable for the first cut of the arachnoid. We held the edge of the incised arachnoid with No. 0 biceps, and made sharp dissections using microscissors (**Figure 2C**). When tension was added in the appropriate direction to open the sulcus, arachnoid trabeculae (**Figure 2D**, white arrow head) appeared between the banks. These were cut sharply with microscissors until the fundus was reached, to make a space for the electrode (**Figures 2E,F**). Importantly, we were careful to withdraw the vessels to the correct side to which they belonged. To avoid venous congestion or brain edema, we never cut or coagulated the veins even if the veins were perfused from both sides.

ELECTRODE ARRAY

We designed a 20-μm-thick Parylene-C-based 128-channel gold electrode array (**Figure 3A**) covering 20 mm × 40 mm for recording from STS (**Figures 3B–D**). The basic structures and fabrication processes of the probe have been described elsewhere (Toda et al., 2011). The probe array contained 8 × 16 electrodes with 2.5-mm inter-electrode spaces. At each electrode, a square of the gold surface was exposed (100 μm × 100 μm; **Figure 3A**, inset). The probe was two-sided comb-like shaped, with eight branches protruding from each side of the main trunk (**Figure 3A**). We also used clinical-use silicone-coated electrode arrays downsized for stimulating the CS in monkeys (**Figure 4**). A double-faced electrode (**Figure 4A**; 1 × 5 array in one side; platinum; 3 mm diameter, 1.5 mm diameter of electrode contact, 5 mm inter-electrode distance with total thickness of 1.2 mm; Unique Medical Co., Tokyo, Japan) was implanted within the CS of two monkeys, while a 20-grid electrode (4 × 5 array; platinum; 3 mm diameter, 1.5 mm diameter of electrode contact, 5 mm inter-electrode distance; Unique Medical Co., Tokyo, Japan) was placed subdurally over the precentral gyrus and postcentral gyrus of one monkey.

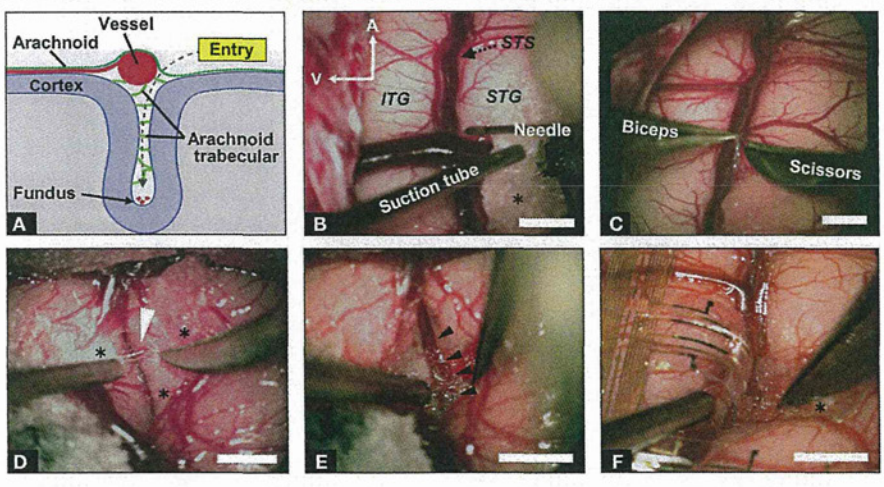

FIGURE 2 | Microdissection for implanting ECoG probe. (A) Schematic illustration of the coronal route of dissection from the entry point to the fundus of the sulcus. **(B)** Microscopic view of the left temporal lobe of the macaque monkey. Microdissection started near the vessels with a 27-gage injection needle. A, anterior; V, ventral; *STS*, superior temporal sulcus; *ITG*, inferior temporal gyrus; *STG*, superior temporal gyrus; asterisk indicates surgical cotton. **(C)** Sharp cutting of the arachnoid membrane. **(D)** Exposure of trabecular connective tissues (white arrowhead) between the upper and lower banks of STS with careful retraction of the lower bank. **(E)** Observation of microvessels at the fundus of the STS (black arrowheads). **(F)** A branch of the electrocorticographic (ECoG) probe inserted into the sulcus. Approximately 7 mm of the probe was inserted in depth. Scale bars indicate 5 mm.

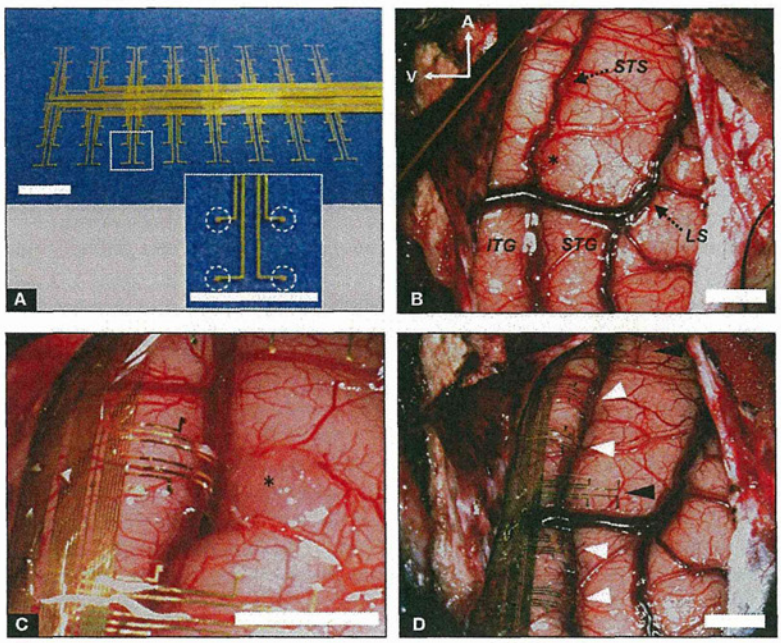

FIGURE 3 | Implantation of recording ECoG probe into STS and ITG. (A) Flexible electrode array to be implanted into STS. Individual electrode contacts are shown in the inset (dotted circles). **(B)** Low-magnification view of the left temporal lobe before probe implantation. STS was dissected from surface to bottom; *LS*, lateral sulcus. **(C)** High-magnification view of probe branches fitted to STS and ITG. **(D)** Low-magnification view of the left temporal lobe following implantation of electrode array. White arrowheads indicate probe branches inserted into STS. Black arrowheads denote branches on the surface of the STG. Scale bars indicate 5 mm.

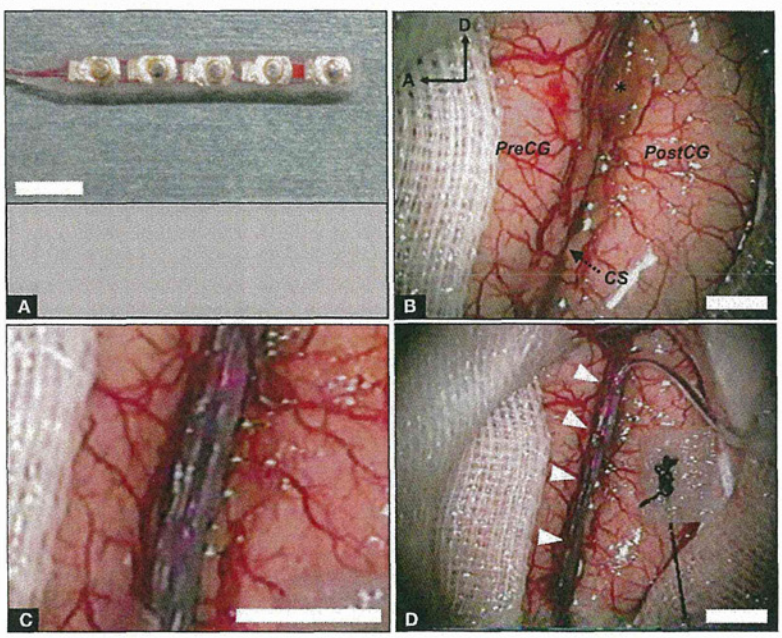

FIGURE 4 | Implantation of stimulating ECoG probe into intrasulcal M1. (A) Double-faced silicone electrode array. **(B)** Photograph of the left fronto-parietal lobes before probe implantation. The CS was dissected from surface to bottom. *PreCG*, precentral gyrus; *PostCG*, postcentral gyrus; A, anterior; D, dorsal; asterisk, surgical cotton. **(C)** High-magnification view of the CS with inserted electrode array. **(D)** Low-magnification view of the CS following implantation of the probe. White arrowheads indicate the bridging veins preserved carefully. Scale bars, 5 mm.

ELECTRODE ARRAY IMPLANTATION

We placed the electrode array carefully into the sulcus, confirming that the probe had not been bent (**Figure 2F**). Importantly, we were careful to fit the electrode array to the brain surface without stress. When there were superficial bridging veins between the banks of the sulcus, we either displaced the electrode's branches to avoid them (**Figure 3D**), or passed the probe under the vessels (**Figure 4D**, white arrow heads). We opened the STS by 30 mm (**Figure 3B**) and a sufficient depth to reach the bottom (5–9 mm). We also opened the CS by 40 mm (**Figure 4B**). We maintained a clear operative field without blood through the surgery to prevent postoperative chemical meningitis.

CLOSING THE CRANIOTOMY

When the implantation of the electrode array was completed, the entire alignment was adjusted again (**Figures 3D and 4D**). The lead was fixed with resin on the bone edge. As the dura shrank during the operation, we patched dural defects using the fascia of the temporal muscle with water-tight suturing to prevent surgical complications such as infection or cerebrospinal fluid leakage. The bone flap was then fixed with a titanium plate and titanium screws. Microconnectors (Omnetics, MN, USA) and a connector chamber (Hokuyo, Niigata, Japan) were fixed strongly also with titanium screws. For the cortical stimulation study, connectors were fixed with resin. We sutured layer by layer and the operation was finished.

RECORDING

Two monkeys (monkey B and F) were trained in a visual fixation task to keep their gaze within ±1° of visual angle of a fixation target (0.3° diameter). Eye movements were captured with an infra-red camera system (i-rec[1]) at a sampling rate of 60 Hz. The stimuli were presented on a 15-inch CRT monitor (NEC, Tokyo, Japan) at a viewing distance of 26 cm. After 450 ms of stable fixation, the stimulus was presented for 300 ms followed by a 600-ms blank interval. Between two and five stimuli were presented successively in a single trial. Monkeys were rewarded with a drop of apple juice for maintaining fixation over the entire duration of the trial. We used 24 photographs of objects from a wide variety of categories, including faces, foods, houses, cars, etc. The long axis of each stimulus subtended 6° of visual angle. For monkey B, stimuli were presented with an x86 PC running a custom-written OpenGL-based stimulation program under Windows XP. Behavioral control for the experiments was maintained by a network of interconnected PCs running QNX real-time OS (QSSL, ON, Canada), which controlled the timing and synchronization. Data was online-monitored and stored on a PC-based system (NSCS, Niigata, Japan). For monkey F, stimuli were presented with a ViSaGe visual stimulus generator (Cambridge Research Systems, Rochester, UK). Task control and data monitoring/storing were maintained by System 3 Real-time Signal Processing Systems (Tucker Davis Technologies, FL, USA).

Electrocorticography signals were differentially amplified using a 128-channel amplifier (Tucker Davis Technologies, FL, USA for monkey F, and Plexon, TX, USA for monkey B) with high- and low-cutoff filters (for monkey B, 300 Hz and 1.0 Hz, respectively; for monkey F, 400 and 1.5 Hz, respectively). All subdural electrodes were referenced to the titanium head restraint post or the titanium connector chamber, which was attached directly to the dura. Signals were recorded at a sampling rate of 1 kHz per channel for monkey B or 2 kHz per channel for monkey F. Signals recorded at 2 kHz were resampled at 1 kHz before the analyses. Electrode impedance was typically 3–5 kΩ. Electrodes with impedance greater than 3 MΩ, possibly due to wiring disconnection at the connector were excluded from the analyses.

For power spectral analysis, data were recorded over a 2-s epoch in each intertrial interval. Data from 96 or 51 two-second epochs were collected from monkey B and F, respectively. The data were segmented into sections, in 256-point windows. Each was Hann-windowed and Fourier transformed with 512 fast Fourier transform (FFT) points. The power spectral density (PSD) was defined as the average over epochs.

The signal-to-noise ratio (SNR) was defined as the ratio of the root mean square (RMS) in the stimulus presentation period to RMS in the prestimulus period in single trials. The data from 50 to 350 ms after onset of the stimulus presentation was used as "signal" and the data from −300 to 0 ms was used as "noise." SNRs were averaged across trials for each channel.

For all analyses, we used in-house Matlab (The MathWorks, MA, USA) codes with the open source Matlab toolbox EEGLAB[2] and R[3].

STIMULATION

Electrical stimulation experiments were conducted under anesthesia, induced with an intramuscular injection of ketamine (10 mg/kg) and maintained with continuous intravenous infusion of propofol (5–10 mg/kg/h) during stimulation. Heart rate and oxygen saturation were continuously monitored. Oxygen saturation was kept over 95%. Body temperature was maintained at 37°C using hot-water bags. Glucose-lactated Ringer's solution was given intravenously (5 ml/kg/h) throughout the experiment. Electrical stimulation was applied in a bipolar fashion to a pair of adjacent electrodes by a programmed digital stimulator (SEN-7103M, Nihon Kohden, Tokyo, Japan) and a stimulus isolator (SS-201J, Nihon Kohden, Tokyo, Japan). Repetitive square-wave electric currents of alternating polarity with a pulse width of 300 μs and a frequency of 50 Hz were delivered for 600 ms. At each electrode site, cortical stimulation began with an amplitude of 0.5 mA, then increased gradually until (1) a maximum of 5 mA was reached or (2) muscle twitches were observed (motor threshold intensity).

HISTOLOGY

At 4 weeks post-implantation, one animal was deeply anesthetized with a sodium pentobarbital overdose (60 mg/kg, i.v.), then transcardially perfused with 1 L of 0.1 M phosphate-buffered saline (PBS) and 2 L of 4% paraformaldehyde in 0.1 M PBS. The brain was removed from the skull and post-fixed at 4°C for 3 days using the same fixative. Samples processed for paraffin embedding were cut into 5 μm sections with a rotary microtome (LR-85, YAMATO KOHKI, Saitama, Japan), The sections were placed on silane-coated glass slides and stained with hematoxylin and eosin.

RESULTS

INTRASULCAL ECoG RECORDING

We implanted a flexible Parylene-C-based gold electrode array (**Figure 3A**) into the ventral bank of the STS and the ITG of the macaque monkey. The STS was successfully opened by 30 mm in

[1]http://staff.aist.go.jp/k.matsuda/eye/doc/i_rec4linuxe.html

[2]http://sccn.ucsd.edu/eeglab/

[3]http://www.r-project.org/

length, and to a sufficient depth to reach the bottom (5–9 mm; **Figures 2E and 3B; Movie S1** in Supplementary Material) by careful dissection under the microscope (**Figure 2**). Eventually, four to five branches of the probe were implanted into the STS (**Figures 3C,D**), whereas other branches and the trunk of the probe were placed on the gyral surface of the ITG. On average, microscopic neurosurgery took approximately 3 h, and there was no postoperative complications.

We recorded visually evoked ECoG signals from two hemispheres of two monkeys that had been trained in a visual fixation task. To evaluate the quality of intrasulcal recording, we compared the ECoG signals from the STS (intrasulcal recording) and ITG (surface recording) in two ways (**Figure 5A**). First, we compared the PSD of the signals. The amplitude of PSD decreased at higher frequencies (**Figure 5B**) in both locations (STS and ITG). The mean PSD for STS tended to be slightly lower than for ITG. There was a significant effect of frequency band (θ, 4–6 Hz; α, 8–12 Hz; β, 16–28 Hz; γ, 32–64 Hz; high γ, 68–100 Hz) on the mean PSD ($p < 10^{-16}$, two-way ANOVA). The effect of location (STS or ITG) did not reach significance ($p = 0.30$), and there was no significant interaction between frequency and location ($p = 0.94$). The normalized power of all the electrodes in two monkeys (**Figure 5C**) revealed no significant difference between STS and ITG in any frequency band (θ, $p = 0.23$; α, $p = 0.41$; β, $p = 0.07$; γ, $p = 0.12$; high γ, $p = 0.20$; Mann–Whitney *U*-test). Second, we compared the SNR of visually evoked potentials (VEPs) from STS and ITG. As shown in **Figure 5D**, the waveform of VEPs was comparable in STS and ITG. SNRs of the single-trial VEP in STS (1.55 ± 0.62, $n = 34$) were not significantly different from those in ITG (1.59 ± 0.62, $n = 176$; $p = 0.73$, *t*-test).

One animal was perfused with paraformaldehyde 4 weeks after surgery. As intended, the flexible probe approached the bottom of the STS at one end, and fitted well to the gyral surface of the ITG at the other end (**Figure 6A**). Close examination of the hematoxylin and eosin stained coronal sections revealed no evidence of microbleeding or physical damage in the implanted regions compared to the control regions (**Figure 6B**).

INTRASULCAL ECoG STIMULATION

We inserted a silicone-coated electrode array into the CS of the monkey. We examined thresholds of intrasulcal M1 stimulation for eliciting individual finger, lip, or wrist movements in comparison with stimulation applied to the gyral surface of M1 (**Figure 7A**). As shown in **Figure 7B**, thresholds with intrasulcal electrical stimulation (1.0 ± 0.2 mA; mean ± SD, $n = 43$) were significantly lower than those with gyral stimulation (3.6 ± 0.4, $n = 50$; $p < 0.001$, *t*-test).

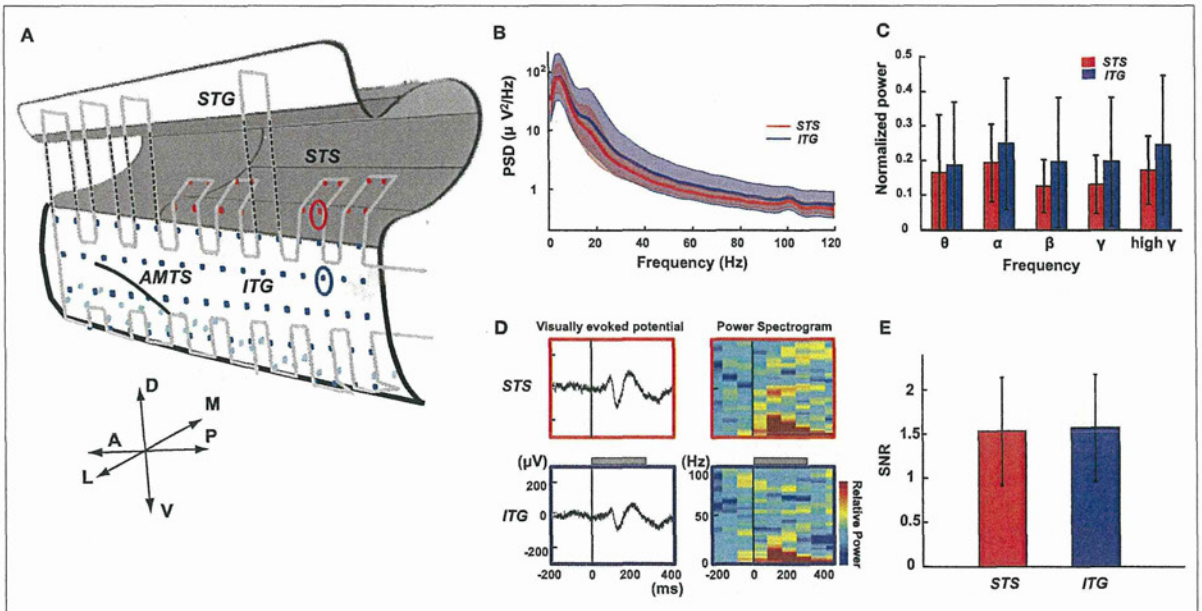

FIGURE 5 | Electrocorticography recording from STS and ITG. (A) Schematic drawing of the left temporal lobe with the electrode array. Dots indicate contacts of the ECoG array covering the STS (red), the lateral part of ITG (blue) and the ventral part of ITG (light blue). Light gray line indicates the outer of the probe. The red and blue circles denote the contact in STS and ITG shown in **(D)**. A, anterior; P, posterior; D, dorsal; V, ventral; L, lateral; M, medial; *AMTS*, anterior middle temporal sulcus. **(B)** Power spectral density (PSD) of ECoG signals from the STS (red) and ITG (blue) during the intertrial interval of a visual fixation task. Solid lines and colored areas indicate mean and standard deviation of PSD, respectively. Data from all the STS ($n = 16$) and ITG ($n = 82$) electrodes in one monkey are included. **(C)** Normalized power of ECoG signals from STS ($n = 34$) and ITG ($n = 176$) for different frequency bands (θ, 4–6 Hz; α, 8–12 Hz; β, 16–28 Hz; γ, 32–64 Hz; high γ, 68–100 Hz). Data are normalized per band by the maximum power of all electrodes in two individual monkeys. Error bars indicate standard deviation across the contacts. **(D)** *Left*: Visually evoked potentials (VEPs) recorded from STS (upper) and ITG (lower). The recording sites are denoted with red (STS) and blue (ITG) circles in **(A)**. A visual stimulus (photograph of a snake) was presented for 300 ms (gray bar). *Right*: The event-related spectrogram of the VEPs (color-coded from −0.4 to +0.4 dB). All responses were averaged for 20 trials. **(E)** Signal-to-noise ratio in STS ($n = 34$) and ITG ($n = 176$) from two individual monkeys. Error bars indicate standard deviation.

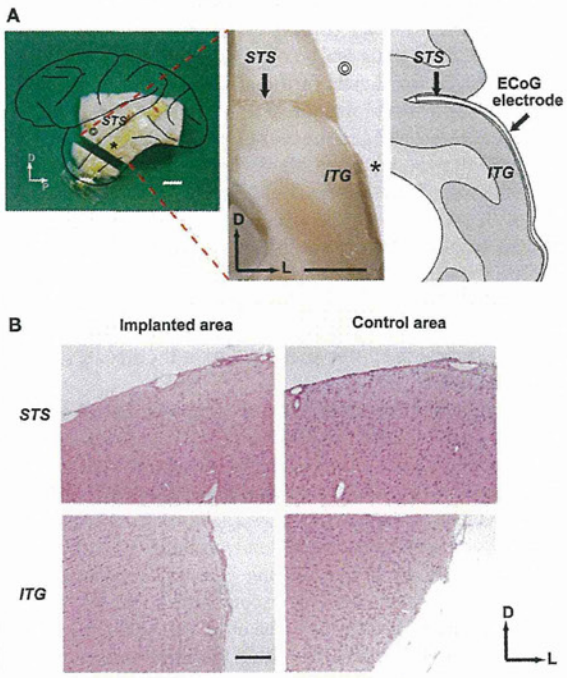

FIGURE 6 | Histological investigation of the ECoG electrode implant. (A) *Left*: Lateral view of the left hemisphere indicating the position of the coronal section shown in the middle. ◎ and * denote STG and ITG, respectively. *Middle*: Coronal cross-section of the brain showing electrode implantation. *Right*: Line drawing of cross-section. Scale bars indicate 5 mm. *P*, posterior; *D*, dorsal; *L*, lateral; *STS*, superior temporal sulcus; *ITG*, inferior temporal gyrus; **(B)** Microscopic view of the coronal sections. The sections from the implanted area of the STS (upper left) and ITG (lower left) as well as the adjacent unimplanted area were stained with hematoxylin and eosin. A scale bar indicates 300 μm.

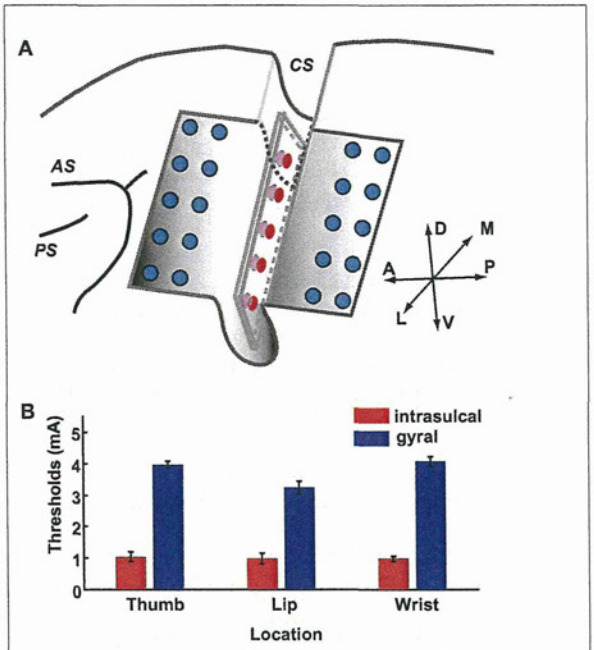

FIGURE 7 | Stimulation thresholds in intrasulcal and gyral M1. (A) Schema of the left frontal lobe with the electrode array. Ten-channel array electrodes (red, five channels in one side) placed between banks of CS were used for intrasulcal cortical stimulation. Ten-channel array electrodes of 20-channel probe (blue) covering precentral gyrus were used for the surface cortical stimulation; *AS*, arcuate sulcus; *PS*, principal sulcus; *CS*, central sulcus. **(B)** Stimulation thresholds of the intrasulcal (red) and gyral (blue) electrodes for motor responses. Bars show the standard deviations.

DISCUSSION

In the present study, we established minimally invasive neurosurgical protocols to place the custom-designed flexible ECoG probe into the cerebral sulcus of the macaque monkey except for the sites where bridging veins were massively growing. To our knowledge, no previous studies have presented data regarding intrasulcal ECoG recording or stimulation in macaque monkeys. Our approach provides an alternative to blind penetration of metal electrodes to the intrasulcal regions, which often cause hemorrhage or secondary epilepsy. It is becoming clear in the neuroprosthetic literature that the use of microelectrodes for the recording of single cell signals that drive artificial effectors has some problems (Polikov et al., 2005; Chao et al., 2010). The main one is the loss of neural signal after long period of time due to the isolation of the electrode's tip by glial cells. The present paper shows a new method that could be a good alternative for neuroprosthetics. In the current study, preservation of normal cortical functions of the implanted region was suggested by (1) equivalent quality of the intrasulcal and the gyral ECoG signals in the temporal cortex and (2) lower stimulation thresholds for intrasulcal M1 stimulation compared to gyral M1 stimulation. Histological examination following perfusion also confirmed minimal damage, if any, due to neurosurgery. Based on our results, we propose that microsurgical protocols, cutting-edge neurosurgical apparatus, and ultra-thin electrode arrays are three key factors critical for avoiding the possible risks of subarachnoid surgery such as ischemia or communicating hydrocephalus, as described in detail in the following three sections.

MICROSURGICAL PROTOCOLS

Compliance with three microsurgical disciplines was essential (Yaargil, 1984–1996). First, we cut the arachnoid trabecular walls or connective tissues sharply. Blunt dissection is not appropriate for this procedure, because it inevitably causes unnecessary tension damaging the pia mater and the underlying neural tissue. Furthermore, we always placed surgical cotton between the pial surface and surgical devices to preserve the cortical surface. Meticulous care must be taken not to directly touch or compress the cortex. Second, during arachnoid dissection, we withdrew the encountered vessels to the correct bank of the sulcus to which they belonged to. The true boundary of both sides was so complicated that ascertainment of the correct plane was required for opening the sulcus widely. These techniques resulted in preserving all of the vessels including the capillaries. Third, we retracted the cortex with biceps or suction tube only

transiently, and never used a brain retractor. Though a retractor can certainly be useful in human brain surgery, in the macaque brain it is difficult to control the position and strength of the retractor in the tiny cerebral sulci. By not using a retractor in the current method, we reduce the risk of local cerebral ischemia that could be caused by long-term retraction. Taken together, these microsurgical protocols are indispensable to preserving the small capillaries and bridging veins, and to maintaining the operative field watery clear.

CUTTING-EDGE NEUROSURGICAL APPARATUS

We introduced two cutting-edge apparatus from human neurosurgery in the present macaque experiments. First, instead of the conventional Horsley–Clarke stereotaxic frame, we developed a three-point free-angle cranial fixation device custom-downsized for the small skull of the macaque in the STS surgery. Without the high flexibility in head positioning, it would be difficult to have direct access to the inferior temporal cortex. In addition, head position was maintained higher than the heart to prevent an increase in intracranial pressure. Although the three-point fixation system could not directly inform the stereotaxic coordinates, a navigation system combining the output of a three-dimensional pointing device onto the structural MRI could enable acquisition of the specific coordinates of the brain during the surgery. Second, we applied a perforator and a craniotome for cranial opening. As in human neurosurgery, the perforator stopped infallibly at the epidural space in macaques, whose skulls are much thinner compared to human skulls. The cortical surface was protected against unintended damage by the tip of craniotome. Compared to the conventional methods of grinding down the skull with a drill in a piecemeal fashion, these apparatus used in our method drastically improved the safety and shortened the time required, so that the cranium can be removed within 1 min. These cutting-edge neurosurgical apparatus are sufficiently versatile for use in various animal model experiments.

ULTRA-THIN FLEXIBLE ELECTRODE

We devised an optimal electrode array for each experiment. For the ECoG recording experiment, we developed an ultra-thin microelectrode array that would not compress the cortex or cause mass effects. The two-sided comb-like structure of the probe might also add flexibility in fitting to the cortical curvature. Our data clearly demonstrated the feasibility of this probe for intrasulcal recording in macaques. This kind of flexible electrode array is expected to become a ubiquitous tool in system neurosciences, because (1) it enables global cortical mapping with high temporal resolution and minimal invasiveness, (2) signal stability is comparable or superior to existing methods (Chao et al., 2010; Toda et al., 2011), and (3) parameters such as the number, size, shape, and intervals of the electrode array can be flexibly adjusted with micrometer resolution for any experimental purpose. In the cortical stimulation experiment in the current study, we modified a clinical-use ECoG probe to reduce its size by half. Although our ultra-thin probe is not suitable for the purpose of electric stimulation at present, we aim to overcome this problem in the near future.

TOWARD WHOLE-BRAIN RECORDING AND STIMULATION

The results of the present recording experiments demonstrated that reliable ECoG signals can be obtained from the intrasulcal cortex, comparable to signals in the adjacent gyral cortex. We employed a simple visual fixation task to evaluate the feasibility of intrasulcal recording in the current protocol. More specific experimental designs to probe higher cognitive functions and detailed analyses in future studies could elucidate the fundamental functional properties of neurons within the sulci. Our stimulation experiment suggested that intrasulcal ECoG could enable us to manipulate the sulcal neural activity *in situ* more precisely and directly compared to remote surface stimulation. Furthermore, the current protocols are basically applicable to other cerebral sulci of the macaque such as the intraparietal sulcus or the arcuate sulcus (unpublished data).

Given that half of the cerebral cortex of the macaque monkey is buried in cerebral sulci, the development of methods for the intrasulcal recording and stimulation is imperative for advancing our understanding of global brain functions (Hackett et al., 2005). Although ECoG is recognized as a well-balanced candidate, the method had been previously applied only to the gyral cortex due to the lack of appropriate non-invasive protocols for the sulcus. The presently proposed technique expands the applicable scope of ECoG to the intrasulcal regions, the other half of the macaque cerebral cortex, and thus provides a way to directly measure and manipulate the activity of the whole brain.

ACKNOWLEDGMENTS

We thank N. Kotake, N. Fujisawa for collaboration in the early phase of the study, A. Honda, M. Takayanagi, A. Kawai, Y. Okawa, K. Abe for technical assistance, and M. Yokoyama, Y. Miyashita for encouragement. This work was supported by VLSI Design and Education Center (VDEC) of The University of Tokyo. The Japanese monkeys used in this research were provided by NBRP "Japanese Monkeys" through the National BioResource Project of the MEXT Japan. This work was supported by Strategic Research Program for Brain Science from the MEXT (Isao Hasegawa, Takafumi Suzuki), 2008 Specified Research grant from Takeda Science Foundation, Toray Science and Technology Grant of Toray Science Foundation (Isao Hasegawa), Grant for Promotion of Niigata University Research Project (Isao Hasegawa), Grant-in-Aid for Scientific Research (C) (Isao Hasegawa), Grant (A) from Hayao Nakayama Foundation for Science and Technology and Culture (Isao Hasegawa), grants from Brain Science Foundation (Isao Hasegawa), and Yujin Memorial Grant of Niigata University (Isao Hasegawa).

SUPPLEMENTARY MATERIAL

The Movie 1 for this article can be found online at http://www.frontiersin.org/Systems_Neuroscience/10.3389/fnsys.2011.00034/abstract

MOVIE S1 | This movie shows an example of the STS operation as described in the text. Craniotomy: Burr holes were opened by a perforator with an attachment for infants (time from 00:00–00:14). The bone and the dura matter were separated using an elevator, the skull then was cut with a craniotome (00:15–00:57). Microsurgery: The surface arachnoid membrane was initially cut near the blood vessel by a 27-gage injection needle. Sharp dissection was made to open the sulcus using microscissors (01:15–01:39). Electrode array was inserted into the sulcus, confirming that the probe had not been bent (01:40–02:06).

REFERENCES

Beauchamp, M. S., Lee, K. E., Argall, B. D., and Martin, A. (2004). Integration of auditory and visual information about objects in superior temporal sulcus. *Neuron* 41, 809–823.

Buschman, T. J., and Miller, E. K. (2007). Top-down versus bottom-up control of attention in the prefrontal and posterior parietal cortices. *Science* 315, 1860–1862.

Chao, Z. C., Nagasaka, Y., and Fujii, N. (2010). Long-term asynchronous decoding of arm motion using electrocorticographic signals in monkeys. *Front. Neuroengineering* 3:3. doi: 10.3389/fneng.2010.00003

Felleman, D. J., and Van Essen, D. C. (1991). Distributed hierarchical processing in the primate cerebral cortex. *Cereb. Cortex* 1, 1–47.

Fisch, L., Privman, E., Ramot, M., Harel, M., Nir, Y., Kipervasser, S., Andelman, F., Neufeld, M. Y., Kramer, U., Fried, I., and Malach, R. (2009). Neural "ignition": enhanced activation linked to perceptual awareness in human ventral stream visual cortex. *Neuron* 64, 562–574.

Hackett, T. A., Karmos, G., Schroeder, C. E., Ulbert, I., Sterbing-D'Angelo, S. J., D'Angelo, W. R., Kajikawa, Y., Blumell, S., and De La Mothe, L. (2005). Neurosurgical access to cortical areas in the lateral fissure of primates. *J. Neurosci. Methods* 141, 103–113.

Hatsopoulos, N. G., and Donoghue, J. P. (2009). The science of neural interface systems. *Annu. Rev. Neurosci.* 32, 249–266.

Koyama, M., Hasegawa, I., Osada, T., Adachi, Y., Nakahara, K., and Miyashita, Y. (2004). Functional magnetic resonance imaging of macaque monkeys performing visually guided saccade tasks: comparison of cortical eye fields with humans. *Neuron* 41, 795–807.

Leuthardt, E. C., Miller, K. J., Schalk, G., Rao, R. P., and Ojemann, J. G. (2006). Electrocorticography-based brain computer interface – the Seattle experience. *IEEE Trans. Neural Syst. Rehabil. Eng.* 14, 194–198.

Liu, H., Agam, Y., Madsen, J. R., and Kreiman, G. (2009). Timing, timing, timing: fast decoding of object information from intracranial field potentials in human visual cortex. *Neuron* 62, 281–290.

Miller, K. J., Sorensen, L. B., Ojemann, J. G., and Den Nijs, M. (2009). Power-law scaling in the brain surface electric potential. *PLoS Comput. Biol.* 5, e1000609. doi: 10.1371/journal.pcbi.1000609

Mountcastle, V. B. (1957). Modality and topographic properties of single neurons of cat's somatic sensory cortex. *J. Neurophysiol.* 20, 408–434.

Polikov, V. S., Tresco, P. A., and Reichert, W. M. (2005). Response of brain tissue to chronically implanted neural electrodes. *J. Neurosci. Methods* 148, 1–18.

Ribas, G. C. (2010). The cerebral sulci and gyri. *Neurosurg. Focus* 28, E2.

Rubehn, B., Bosman, C., Oostenveld, R., Fries, P., and Stieglitz, T. (2009). A MEMS-based flexible multichannel ECoG-electrode array. *J. Neural Eng.* 6, 036003.

Slutzky, M. W., Jordan, L. R., Krieg, T., Chen, M., Mogul, D. J., and Miller, L. E. (2010). Optimal spacing of surface electrode arrays for brain–machine interface applications. *J. Neural Eng.* 7, 26004.

Toda, H., Suzuki, T., Sawahata, H., Majima, K., Kamitani, Y., and Hasegawa, I. (2011). Simultaneous recording of ECoG and intracortical neuronal activity using a flexible multichannel electrode-mesh in visual cortex. *Neuroimage* 54, 203–212.

Tomita, H., Ohbayashi, M., Nakahara, K., Hasegawa, I., and Miyashita, Y. (1999). Top-down signal from prefrontal cortex in executive control of memory retrieval. *Nature* 401, 699–703.

Tsao, D. Y., Freiwald, W. A., Knutsen, T. A., Mandeville, J. B., and Tootell, R. B. (2003). Faces and objects in macaque cerebral cortex. *Nat. Neurosci.* 6, 989–995.

Yaargil, M. G. (1984–1996). *Microneurosurgery*. New York: Georg Thieme Verlag.

Yanagisawa, T., Hirata, M., Saitoh, Y., Kato, A., Shibuya, D., Kamitani, Y., and Yoshimine, T. (2009). Neural decoding using gyral and intrasulcal electrocorticograms. *Neuroimage* 45, 1099–1106.

Conflict of Interest Statement: The authors declare that the research was conducted in the absence of any commercial or financial relationships that could be construed as a potential conflict of interest.

Received: 19 April 2011; accepted: 12 May 2011; published online: 25 May 2011.
Citation: Matsuo T, Kawasaki K, Osada T, Sawahata H, Suzuki T, Shibata M, Miyakawa N, Nakahara K, Iijima A, Sato N, Kawai K, Saito N and Hasegawa I (2011) Intrasulcal electrocorticography in macaque monkeys with minimally invasive neurosurgical protocols. Front. Syst. Neurosci. 5:34. doi: 10.3389/fnsys.2011.00034

British Journal of Neurosurgery, April 2011; 25(2): 197–202

informa
healthcare

ORIGINAL ARTICLE

Refined analysis of complex language representations by non-invasive neuroimaging techniques

TAKAHIRO OTA[1], KYOUSUKE KAMADA[1], KENSUKE KAWAI[1], MASATO YUMOTO[2], SHIGEKI AOKI[3] & NOBUHITO SAITO[1]

[1]*Department of Neurosurgery, The University of Tokyo, Tokyo, Japan,* [2]*Department of Clinical Laboratory, The University of Tokyo, Tokyo, Japan, and* [3]*Department of Radiology, The University of Tokyo, Tokyo, Japan*

Abstract

Objective. The determination of language lateralisation is important for patients with medically intractable epilepsy or a brain tumour near the language areas to avoid the risk of post-surgical language deficits. The aim of this study was to evaluate the clinical usefulness of near-infrared spectroscopy (NIRS) to identify language lateralisation compared with functional MRI (fMRI) and magnetoencephalography (MEG) in multiple language tasks.

Methods. We investigated 28 patients whose language dominance was evaluated by the Wada test. fMRI, MEG and NIRS were performed to investigate language representation. All patients were as'ked to read three-letter words silently for fMRI and MEG (*Kana* reading) and to write words beginning with a visually presented letter (word generation) for NIRS. The laterality index was calculated to assess language lateralisation in each investigation.

Results. In 24 cases (85.7%), of which two investigations showed the same laterality, the results had perfect concordance with the Wada test. In patients with left dominance, the sensitivity and specificity of fMRI, MEG and NIRS was 95.0% and 62.5%, 100% and 87.5%, 75.0% and 87.5%, respectively. In three patients with right lateralization, only NIRS showed a significant increase of oxygenated-haemoglobin in the right inferior frontal region, indicating right dominance.

Conclusion. We established a method to determine language lateralisation by co-utilising fMRI, MEG and NIRS with high reliability. NIRS recognised atypical language representation, in addition to fMRI and MEG. While fMRI, MEG and NIRS are not currently as accurate as the Wada test in determining language lateralisation, this non-invasive and repeatable method has great potential as an alternative to the Wada test in time following further research and refinement of these techniques.

Key words: *Functional MRI, magnetoencephalography, near-infrared spectroscopy, language lateralisation.*

Introduction

The determination of language lateralisation is important for patients with medically intractable epilepsy or brain tumour near the language areas to avoid risks of post-surgical language deficits.[1] The Wada test has been widely accepted to determine the hemispheric dominance of language-related functions;[2] however, it includes several risks related to angiography[3] and is not easily repeatable for neurosurgical operation candidates.

Because of the rapid development of imaging techniques, functional MRI (fMRI) has become popular in clinical use. Many neurosurgical institutes have high-field MR scanners, equipped with fMRI sequences. Data acquisition and processing in fMRI are relatively simple and much safer than the Wada test; therefore, several reports have assessed language lateralisation by fMRI since 1996,[4] although the overall concordance rate between fMRI and the Wada test did not reach 90%.[4,5] According to previous studies, fMRI markedly failed to indicate atypical (right and bilateral) language representation.[6]

The other option for this purpose is magnetoencephalography (MEG). This new technology directly measures neurophysiological activity and has millisecond-order high temporal resolution compared to fMRI (second-order). Papanicolaou *et al.* and Simos *et al.* established processes to determine hemispheric language lateralisation by counting the number of dipoles related to language tasks in each hemisphere;[7,8] however MEG is also not ideal to identify lateralisation, especially in cases of reduced cognitive capacity.[9]

Several studies have recently adapted near-infrared spectroscopy (NIRS) to detect language-related functions.[10] NIRS has not been clinically acknowledged for human brain mapping in neurosurgical patients.

Correspondence: Kyousuke Kamada, M.D., Ph.D., School of Medicine, Asahikawa Medical University 2-1, Midorigaoka-Higashi, Asahikawa, Hokkaido, 078-8510, Japan. Tel: +81-166-68-2594. Fax: +81-166-68-2599. E-mail: kamady-k@umin.ac.jp

Received for publication 1 December 2009. Accepted 29 June 2010.

ISSN 0268-8697 print/ISSN 1360-046X online © 2011 The Neurosurgical Foundation
DOI: 10.3109/02688697.2010.505986

Three studies of NIRS, however, demonstrated the positive potential to indicate language lateralisation.[11] Although the procedures have not been well established, this technique has several advantages over other imaging modalities. First, it monitors continuous concentration changes of oxygenated-haemoglobin (Oxy-Hb) and deoxygenated-haemoglobin (Deoxy-Hb) independently. Second, the equipment is portable and less costly than MR scanners. The most important benefit of NIRS in clinical practice is that this system needs no major restrictions on movement or vocalisation during measurement. We, therefore, expect that NIRS might have great potential for preoperative evaluation in neurosurgery. Functional transcranial Doppler is a reasonable alternative for lateralisation of language dominance, but it requires additional validation, particularly with patients who have atypical language representations.[12,13]

To our knowledge, no study has employed these three modalities for refined analysis of complex language representation in neurosurgical patients. The aim of this study was to evaluate the clinical usefulness of NIRS to identify language lateralisation, comparing with fMRI and MEG in several language tasks. The findings of 28 neurosurgical patients were carefully analysed based on the results of the Wada test. The Wada test assesses both language and memory-related functions;[14] however, in this article only the language part of the test is under consideration.

Patients

The patients were all native Japanese speakers, 12 males and 16 females with a median age of 37.3 years old (range 14–74). fMRI, MEG and NIRS were performed in all 28 patients, who underwent the Wada test to validate hemispheric dominance. The handedness of all patients was assessed by the Edinburgh Handedness Inventory.[15] Thirteen, 13 and 2 patients had medically intractable epilepsy, brain tumour and arteriovenous malformation (AVM), respectively. The demographic data of the patients are presented in Table I. Tumour patients had little difficulty in communicating, except case 24, who suffered from mild dysarthria. All epilepsy patients underwent a neuropsychological examination (Japanese Wechsler Adult intelligence Scale-Revised (Wechsler, 1990)) to evaluate their cognitive status, including language acuity.

This study was approved by our institutional review board, and written informed consent was obtained from each subject before participation.

TABLE I. Demographic data of all patients

Case	Age/ Sex	Diagnosis	Location	Handedness	Verbal IQ
1	16F	Meningioma	Left temporal	Left	N.T.
2	26F	Epilepsy	Right temporal	Left	87
3	24M	Epilepsy	Left temporal	Left	83
4	18F	AVM	Left frontal	Left	N.T.
5	45M	Glioma	Left temporal	Right	N.T.
6	48M	Glioma	Left parietal	Right	N.T.
7	39F	Glioma	Right frontal	Right	N.T.
8	36F	Glioma	Right insula	Right	N.T.
9	45F	CM	Left thalamus	Right	N.T.
10	14M	Glioma	Left temporal	Right	68
11	74M	Meningioma	Left temporal	Right	N.T.
12	39M	Glioma	Right frontal	Right	N.T.
13	49F	Epilepsy	Right temporal	Right	91
14	15F	Epilepsy	Left temporal	Right	115
15	40M	Epilepsy	Left temporal	Right	85
16	36F	Epilepsy	Left temporal	Right	71
17	37F	Epilepsy	Left temporal	Right	94
18	40M	Epilepsy	Right temporal	Right	93
19	47F	Epilepsy	Right temporal	Right	88
20	34F	Epilepsy	Left temporal	Right	123
21	57F	Meningioma	Left petrous	Right	N.T.
22	56M	Glioma	Right insula	Right	N.T.
23	27F	AVM	Left occipital	Right	N.T.
24	66M	Glioma	Left frontal	Right	N.T.
25	25M	Epilepsy	Left temporal	Right	68
26	31F	Epilepsy	Right temporal	Right	79
27	29M	Epilepsy	Left temporal	Right	74
28	30F	Glioma	Left frontal	Right	N.T.

M: Male, F: Female, IQ: intelligence quotient, AVM: arteriovenous malformation, CM: cavernous malformation, N.T.: not tested.

Methods

Language fMRI

All MR imaging was performed with a 3 tesla MR scanner (Signa 3.0T HDx System; GE Healthcare, USA). fMRI was performed with a T2*-weighted echo planar imaging sequence (TE 35 msec; TR 4000 msec; flip angle 90°; slice thickness 2.5 mm; slice gap 1 mm; field of view 240 mm; matrix 64 × 64; 24 slices). We used a reading task (*Kana* reading task) to indicate language-related functions. Words consisting of three *Kana* letters (Japanese phonetic symbols as the alphabet) were presented on a liquid crystal display monitor with a mirror above the head coil allowing the patients to see the words. Patients were instructed to categorise the presented word silently into 'abstract' or 'concrete' based on the nature of the word. During interval periods, patients passively viewed random dots of destructured *Kana* letters that were controlled to have the same luminance as the stimuli to eliminate primary visual responses. After data acquisition, functional activation maps were calculated by estimating *Z*-scores between rest and activation periods using Dr. View (Asahi Kasei, Japan). Pixels with *Z*-scores higher than 2.2 ($p < 0.05$) were considered to indicate real activation and were used for mapping. Further details of data acquisition and data analysis have been described elsewhere.[16]

After counting the total number of activated pixels in the inferior frontal gyrus (IFG) and the middle frontal gyrus (MFG), the laterality index (LI) of the activated pixels of left (L) and right (R) hemispheres